Neuroradiology (2021) 63:1709–1719
https://doi.org/10.1007/s00234-021-02758-z

HEAD-NECK-ENT RADIOLOGY

Quantitative dynamic contrast-enhanced MRI and readout segmentation of long variable echo-trains diffusion-weighted imaging in differentiating parotid gland tumors

Nan Huang[1] · Zebin Xiao[2] · Yu Chen[1] · Dejun She[1] · Wei Guo[1] · Xiefeng Yang[1] · Qi Chen[1] · Dairong Cao[1] · Tanhui Chen[1]

Received: 20 March 2021 / Accepted: 20 June 2021 / Published online: 9 July 2021

Abstract

Purpose To evaluate the ability of quantitative dynamic contrast-enhanced (DCE)-MRI and readout segmentation of long variable echo-trains diffusion-weighted imaging (RESOLVE-DWI) in differentiating parotid tumors (PTs) with different histological types.

Methods In this retrospective study, 123 patients with 145 histologically proven PTs who underwent both RESOLVE-DWI and DCE-MRI were enrolled including 51 pleomorphic adenomas (PAs), 52 Warthin's tumors (WTs), 27 other benign neoplasms (OBNs), and 15 malignant tumors (MTs). Quantitative parameters of DCE-MRI (K^{trans}, K_{ep}, and V_e) and the apparent diffusion coefficient (ADC) of lesions were calculated and analyzed. Kruskal–Wallis tests with Dunn-Bonferroni correction, logistic regression analyses, and receiver operating characteristic curve were used for statistical analyses.

Results PAs exhibited a lowest K^{trans} among these four PTs. WTs demonstrated the highest K_{ep} and lowest V_e values. WTs and MTs showed lower ADC_{min} values than PAs and OBNs. The combination of K_{ep} and V_e provided 98.1% sensitivity, 85% specificity, and 98.7% accuracy for differentiating WTs from the other three PTs. The ADC_{min} cutoff value of ≤ 0.826 yielded 80.0% sensitivity, 92.3% specificity, and 90.3% accuracy for the differentiation of MTs from PAs and OBNs. K^{trans} with a cutoff value of ≤ 0.185 achieved a sensitivity, specificity, and accuracy of 84.3, 70.4, and 79.5%, respectively, for discriminating PAs from OBNs.

Conclusion The combination of quantitative DCE-MRI and RESOLVE-DWI is beneficial for characterizing four histological types of PTs.

Keywords Parotid tumor · Magnetic resonance imaging · DCE-MRI · RESOLVE-DWI · Perfusion · Diffusion

Introduction

Parotid tumors (PTs) account for 85% of salivary tumors and involve a wide range of benign and malignant lesions [1]. The differentiation of different types of PTs is of great clinical relevance as treatment options and prognosis differ among different histologic types. Specifically, pleomorphic adenomas (PAs) and Warthin's tumors (WTs) are the most common types of benign PTs [2], and PAs are associated with a higher risk for relapse and malignant transformation than WTs and other benign neoplasms (OBNs) [3]. Malignant parotid tumors (MTs) consisting 20% of PTs usually have a high potential for recurrence and poor prognosis [2]. Based on their biological behavior, limited partial parotidectomy [4] or enucleation [5] is preferred for WTs and OBNs in clinic, while complete and larger free resection margins are recommended for PAs and MTs [3, 6, 7]. Clinically, fine needle aspiration biopsy is required to confirm the diagnosis of PTs; however, it may result in tumor spillage in PAs or metastasis in MTs. Therefore, non-invasive imaging techniques, such as CT and MR imaging (MRI), play an important role in differential diagnosis of PTs. Nevertheless,

Nan Huang and Zebin Xiao contributed equally to this work.

✉ Tanhui Chen
chenth0629@sina.com

[1] Department of Radiology, First Affiliated Hospital of Fujian Medical University, 20 Cha-Zhong Road, Fuzhou, Fujian 350005, People's Republic of China

[2] Department of Biomedical Sciences, University of Pennsylvania, Philadelphia, PA 19104, USA

different types of PTs cannot be easily discriminated because of their overlapping imaging features [8–10].

Advanced MRI approaches, especially semi-quantitative dynamic contrast-enhanced (DCE)-MRI and single-shot echo-planar imaging (SS-EPI) diffusion-weighted imaging (DWI), have been proven to be helpful in the differentiation of PTs [11–14]. However, substantial overlap of time-intensity curve (TIC) and apparent diffusion coefficient (ADC) values as well as conflicting results among different studies do exist [14–16]. Moreover, semi-quantitative DCE-MRI parameters can be influenced by tissue relaxation times, contrast agent registration protocol, and imaging parameters [17]. In addition, SS-EPI-DWI used in these studies suffer from the geometric distortion [18] and artifacts in the head and neck [19, 20].

Quantitative DCE-MRI measures the contrast agent exchange between the intravascular and the extravascular space to quantify tissue perfusion and permeability based on pharmacokinetic analysis [17, 21, 22]. Although a few studies reported the usefulness of quantitative DCE-MRI in the discrimination of PTs, they still have some intrinsic shortcomings, such as small sample size or low temporal resolution [23–25]. Readout segmentation of long variable echo-trains diffusion-weighted imaging (RESOLVE-DWI) divides the readout into multiple k-space segments to shorten the echo spacing, which permits a reduction in geometric distortion and susceptibility artifacts [20], and produces more homogeneous images and higher signal-to-noise resolution than SS-EPI-DWI [19, 26, 27]. Moreover, ADC value derived from RESOLVE-DWI might be more accurate [28–30]. A few studies pointed out that ADC histogram analysis using RESOLV-DWI was effective in differentiating common PTs, but their sample size was still small [31, 32].

To the best of our knowledge, no studies have been reported in the characterization of PTs with the combination of quantitative DCE-MRI and RESOLVE-DWI. Thus, the purpose of our study was to evaluate whether the combination of quantitative DCE-MRI and RESOLVE-DWI was effective for differentiating PAs, WTs, OTBs, and MTs.

Subjects and methods

Study sample

Our retrospective study was approved by the institutional review board in our hospital, with informed consent waived due to the retrospective nature of this study. Potentially eligible patients with histologically confirmed PTs between August 2016 and October 2019 were identified. Inclusion criteria were the following: (1) patients who underwent both DCE-MRI and RESOLVE-DWI; (2) tumors with maximum diameter > 1 cm; (3) enough noncystic/nonnecrotic areas within the tumors for imaging analysis; and (4) good quality of MR images without severe motion or susceptibility artifacts. Patients with presence of cyst (i.e., branchial cleft cyst and lymphoepithelial cyst), lipomyoma, or lymphangioma reliably diagnosed by clinical and radiological methods and patients who had biopsy or surgery less than 2 weeks before MR examination were excluded from the study. Finally, a total of 123 patients (mean age, 49.2 years; age range, 16–78 years) with 145 histologically proven PTs including 51 tumors with PAs, 52 tumors with WTs, 15 tumors with MTs, and 27 tumors with OBNs were enrolled in this study. The MTs included mucoepidermoid carcinoma ($n = 6$), acinar cell carcinoma ($n = 2$), duct carcinoma ($n = 2$), lymphoma ($n = 2$), carcinoma ex pleomorphic adenoma ($n = 1$), mammary analogue secretory carcinoma ($n = 1$), and fibrosarcoma ($n = 1$). Other benign tumors included basal cell adenoma ($n = 18$), schwannoma ($n = 5$), oncocytoma ($n = 1$), cystadenoma ($n = 1$), myoepithelioma ($n = 1$), and hemolymphangioma ($n = 1$).

MRI protocol

The MRI examinations were performed on a 3 T Siemens Skyra scanner (Siemens Healthcare, Erlangen, Germany) using a 20-channel head and neck coil. The routine imaging protocols included axial T1-weighted MRI (repetition time/echo time [TR/TE], 739/9.9 ms; field of view [FOV], 220 × 206 mm; matrix, 320 × 256; slice thickness, 4 mm; flip angles [FA] = 128°), axial T2-weighted MRI (TR/TE, 3690/83 ms; FOV, 220 × 220 mm; matrix, 320 × 320; slice thickness, 4 mm; FA = 100°), sagittal T1-weighted MRI (TR/TE, 725/8.4 ms; FOV, 300 × 225 mm; matrix, 320 × 240; slice thickness, 4 mm; FA = 120°), coronal T1-weighted MRI (TR/TE, 725/8.4 ms; FOV, 280 × 228 mm; matrix, 320 × 240; slice thickness, 3 mm; FA = 120°), and coronal T2WI (TR/TE, 4000/82 ms; FOV, 280 × 228 mm; matrix, 320 × 256; slice thickness, 3 mm; FA = 160°).

The RESOLVE-DWI using a readout segmented echo planar imaging, parallel imaging (GRAPPA), and a two-dimensional navigator-based reacquisition in 3-scan trace direction was performed. The imaging parameters were as follows: TR/TE, 3860/60 ms, FOV, 220 × 220 mm; matrix, 150 × 150; slice thickness, 4 mm; number of slices, 20; parallel imaging acceleration factor, 2; FA = 180°; bandwidth, 926 Hz/Px; intersection gap, 0.2 mm; readout segments, 5; echo spacing, 0.36 ms; and b values, 50 and 800 s/mm^2. The acquisition time of the RESOLVE-DWI was 2 min and 31 s.

T1 mapping was performed initially followed by DCE-MRI sequence. The T1 mapping parameters included TR/TE, 4.95/1.75 ms; FOV, 240 × 100 mm; matrix, 192 × 154; and slice thickness, 2 mm, FA = 2°/15°. The imaging parameters of DCE-MRI included TR/TE, 5.08/1.79 ms; FOV, 240 × 217 mm, acquisition matrix, 192 × 154, intersection

gap, 0, slice thickness, 3.5 mm, slice number, 20; temporal resolution, 6–6.9 s/dynamic, number of dynamics, 35–50; and FA = 15°, number of excitations [NEX] = 1. For the dynamic acquisitions, gadopentetate dimeglumine (Gd-DTPA, MultiHance, Bracco Diagnostics) at a dose of 0.1 mmol/kg body weight was injected intravenously with a power injector at a flow rate of 2 ml/s followed by 15 ml of 0.9% saline flush. The acquisition time of the DCE-MRI was 3 min and 48 s–5 min.

Image processing and assessment

The DCE-MRI were processed by a semi-automatic software Tissue 4D (Syngo.via; Siemens Healthcare) and pharmacokinetic evaluation was based on the Tofts model. After motion correction and image registration, volume of interest (VOI) containing the lesion was drawn to obtain a time-signal-intensity curve on which the arrival time of contrast agent was determined. An appropriate arterial input function (AIF) was set and then the time-concentration curve from the VOI and parameter maps were generated. Measurements of the K^{trans} (inflow rate constant of the constant agent between plasma and the extravascular extracellular space [33]), K_{ep} (reverse rate constant of contrast agent between EES and plasma), and V_e (volume fraction of the EES) values were performed with a free-hand-mode ROI. With reference to T2-weighted and contrast-enhanced T1-weighted images to avoid obvious hemorrhagic, necrotic regions, or cystic-appearing areas as much as possible, the ROI was manually outlined along the outer margin of enhancing area on the largest enhancing slices with maximal enhancement on the parameter map. The mean K^{trans}, K_{ep}, and V_e values were derived.

Apparent diffusion coefficient (ADC) maps of the RESOLVE-DWI were reconstructed in the scanner using the monoexponential model, and measurement of ADC was conducted in picture archiving and communication systems. The measurement of ADC value was conducted with the same ROIs as used in the measurements of DCE parameters first (ADC_{ROI}), and then 5 small round ROI (range, 0.03–0.05 cm^2) were placed within the former ROI and the lowest ADC value was selected as ADC_{min}.

The measurement of DCE-MRI (K^{trans}, K_{ep}, and V_e) and RESOLVE-DWI (ADC_{ROI} and ADC_{min}) parameters were performed in a blind manner by two radiologists (N.H. and Y.C, with 8 and 2 years' experience, respectively, in head and neck imaging) independently. For evaluation of inter- and intra-observer reproducibility, the measurement was obtained by readers 1 and 2 and was repeated by reader 1 with a minimum 1-month washout period. The average of measurements of reader 1 and reader 2 was taken for statistical analysis.

Statistical analysis

Statistical analyses were performed using SPSS 24.0 software (IBM, Chicago) and MedCalc statistical software version 15.8; (MedCalc Software bvba, Ostend, Belgium). The inter- and intra-observer reproducibility for DCE and RESOLVE-based ADC parameter measurements were assessed with the intraclass correlation coefficient (ICC) with 95% confidence interval. An ICC > 0.75 was considered as a good agreement. For each parameter, Kolmogorov–Smirnov Normality test was performed to assess normal data distribution and Levene's test was performed to test variance homogeneity. All RESOLVE-DWI and DCE-MRI parameters of the PTs are presented as the mean ± standard deviation. Mann–Whitney U test was used for the comparisons of benign and malignant PTs. Kruskal–Wallis tests with Dunn-Bonferroni correction were applied for multiple comparisons of all parameters among PAs, WTs, OTBs, and MTs. The receiver operating characteristic curve (ROC) analyses were established to evaluate the diagnostic performances and determine optimum cutoff value of K_{ep} and V_e for the discrimination of WTs from the group of PAs + OBNs + MTs, of ADC_{min} for the discrimination of MTs from the group of PAs + OBNs, and of K^{trans} and K_{ep} for the discrimination of PAs from OBNs with MedCalc statistical software. The optimal cutoff values were determined using the Youden index to maximize sensitivity and specificity. Based on optimum cutoff values, the area under the curve (AUC), sensitivity, specificity, positive predictive value, negative predictive value, and accuracy were calculated for each parameter. The significant parameters achieving the highest Youden index were further included for stepwise differential diagnosis of these four groups of PTs. The combination of K_{ep} and V_e values for the discrimination of WTs from the group of PAs + OBNs + MTs was based on logistic regression analysis in MedCalc software. Comparisons of the AUC were performed. P values < 0.05 were statistically significant.

Validation study

To validate the diagnostic accuracy of the stepwise protocol, 5 consecutive patients (mean age, 51.4 years; age range, 28–79 years) from March 2020 to November 2020 who underwent both RESOVE-DWI and DCE-MRI were enrolled to perform the validation study. The Inclusion criteria and technique were the same as described previously. They included PA ($n = 1$), WT ($n = 1$), MTs ($n = 2$), and OBN ($n = 1$).

Results

DCE-MRI and RESOLVE-DWI analysis

Table 1 summarized detailed quantitative DCE-MRI parameters and ADC values of benign and malignant tumors. The ADC_{min} of benign tumors ($[0.932 \pm 0.400] \times 10^{-3}$ mm^2/sec) was significantly higher than malignant tumors ($[0.703 \pm 0.231] \times 10^{-3}$ mm^2/sec) ($P = 0.037$). No significant differences were found in K^{trans}, K_{ep}, V_e, and ADC_{ROI} between the benign and malignant groups.

The K^{trans}, K_{ep}, V_e, ADC_{ROI}, and ADC_{min} values of different histological types of PTs are summarized in Table 2. Subgroup comparisons of all parameters among PAs, WTs, OBNs, and MTs are shown in Fig. 1. The mean K^{trans} value of PAs was significantly lower than that of WTs, OBNs, and MTs (both adjusted $P < 0.001$ for WTs and OBNs, and adjusted $P = 0.019$ for MTs). Compared with PAs, OBNs, and MTs, significantly higher mean K_{ep} and lower mean V_e values were found in WTs (all adjusted $P < 0.001$). The mean K_{ep} value of PAs was significantly lower than that of OBNs (adjusted $P < 0.01$). The mean ADC_{ROI} and ADC_{min} values of PAs were significantly higher than those of WTs and MTs (both adjusted $P < 0.001$), and the mean ADC_{ROI} and ADC_{min} value of WTs were significantly lower than those of PAs and OBNs (both adjusted $P < 0.001$). Furthermore, significantly lower mean ADC_{min} value was found in MTs compared with OBNs (adjusted $P = 0.017$).

Excellent inter- and intra-observer agreement was achieved in quantitative measurements for K^{trans}, K_{ep}, V_e, ADC_{ROI}, and ADC_{min} values with ICCs ranging from 0.932 to 0.98 (Table 3).

Table 1 Comparisons of K^{trans}, K_{ep}, V_e, ADC_{min} and ADC_{ROI} values between benign and malignant parotid tumors (Mean ± SD)

Parameters	Benign ($n = 130$)	Malignant ($n = 15$)	P
DCE parameters			
K^{trans}(/min)	0.262 ± 0.196	0.244 ± 0.159	.874
K_{ep}(/min)	1.275 ± 1.255	0.776 ± 0.565	.370
V_e	0.292 ± 0.163	0.338 ± 0.101	. 050
DWI parameters			
ADC_{ROI} ($\times 10^{-3} mm^2/s$)	1.229 ± 0.446	1.046 ± 0.288	.203
ADC_{min} ($\times 10^{-3} mm^2/s$)	0.932 ± 0.400	0.703 ± 0.231	.037**

Except for the p values, data are presented as mean ± standard deviation. Data in parentheses indicates the number of corresponding patients

K^{trans} volume transfer constant, K_{ep} reverse rate constant, V_e fractional volume in the EES, ADC_{ROI} the apparent diffusion coefficient of corresponding ROI in DCE parameter measurements, ADC_{min} the minimum apparent diffusion coefficient of 5 small round ROI (ranging 0.03–0.05 cm^2) within the former ROI in ADC_{ROI} measurement

Stepwise discrimination of four groups of parotid tumor using RESOLVE-DWI and DCE-MRI

The results of the ROC curve analysis that summarized the sensitivity, specificity, PPV, NPV, accuracy, and AUC for stepwise differentiation between four PTs are shown in Table 4.

First, PAs, OBNs, and MTs were grouped together, as significant differences of K_{ep} and V_e values were observed between these three tumors and WTs. The ROC analyses revealed that a cutoff K_{ep} value of 1.016 provided 94.2% sensitivity, 83.9%specificity, and 87.6% accuracy; a cutoff V_e value of 0.257 provided 92.3% sensitivity, 79.6% specificity, and 81.1% accuracy. The combination of K_{ep} and V_e was performed further, and the model produced by logistic regression analysis was as follows: Logit (P) = $2.825 \times K_{ep} - 30.233 \times V_e + 3.0256$; combination = $V_e \times 30.233/2.825 - K_{ep}$. ROC analyses yielded that the combination of K_{ep} and V_e with a cutoff value of 0.169, achieved the highest Youden index of 0.830, with 98.1% sensitivity, 85% specificity, and 89.7% accuracy for the differentiation between WTs and the group of PAs + OBNs + MTs (Table 4 and Fig. 2a).

Table 2 RESOLVE-DWI and DCE-MRI characteristics of pleomorphic adenomas, Warthin's tumors, other benign neoplasms, and malignant tumors (Mean ± SD)

Parameters	PA($n = 51$)	OBN($n = 27$)	WT($n = 52$)	MT($n = 15$)
DCE parameters				
K^{trans} (/min)	0.129 ± 0.121	0.294 ± 0.194	0.375 ± 0.181	0.244 ± 0.159
K_{ep} (/min)	0.406 ± 0.422	0.943 ± 0.623	2.299 ± 1.312	0.776 ± 0.565
V_e	0.380 ± 0.192	0.341 ± 0.102	0.181 ± 0.065	0.338 ± 0.101
DWI parameters				
ADC_{ROI} ($\times 10^{-3} mm^2/s$)	1.600 ± 0.316	1.376 ± 0.269	0.790 ± 0.149	1.046 ± 0.288
ADC_{min} ($\times 10^{-3} mm^2/s$)	1.266 ± 0.315	1.037 ± 0.226	0.550 ± 0.124	0.703 ± 0.231

K^{trans} volume transfer constant, K_{ep} reverse rate constant, V_e fractional volume in the EES, ADC_{ROI} the apparent diffusion coefficient of corresponding ROI in DCE parameter measurements, ADC_{min} the minimum apparent diffusion coefficient of 5 small round ROI (ranging 0.03–0.05cm^2) within the former ROI in ADC_{ROI} measurement, *PA* pleomorphic adenomas, *OBN* other benign neoplasms, *WT* Warthin's tumors, *MT* malignant tumors

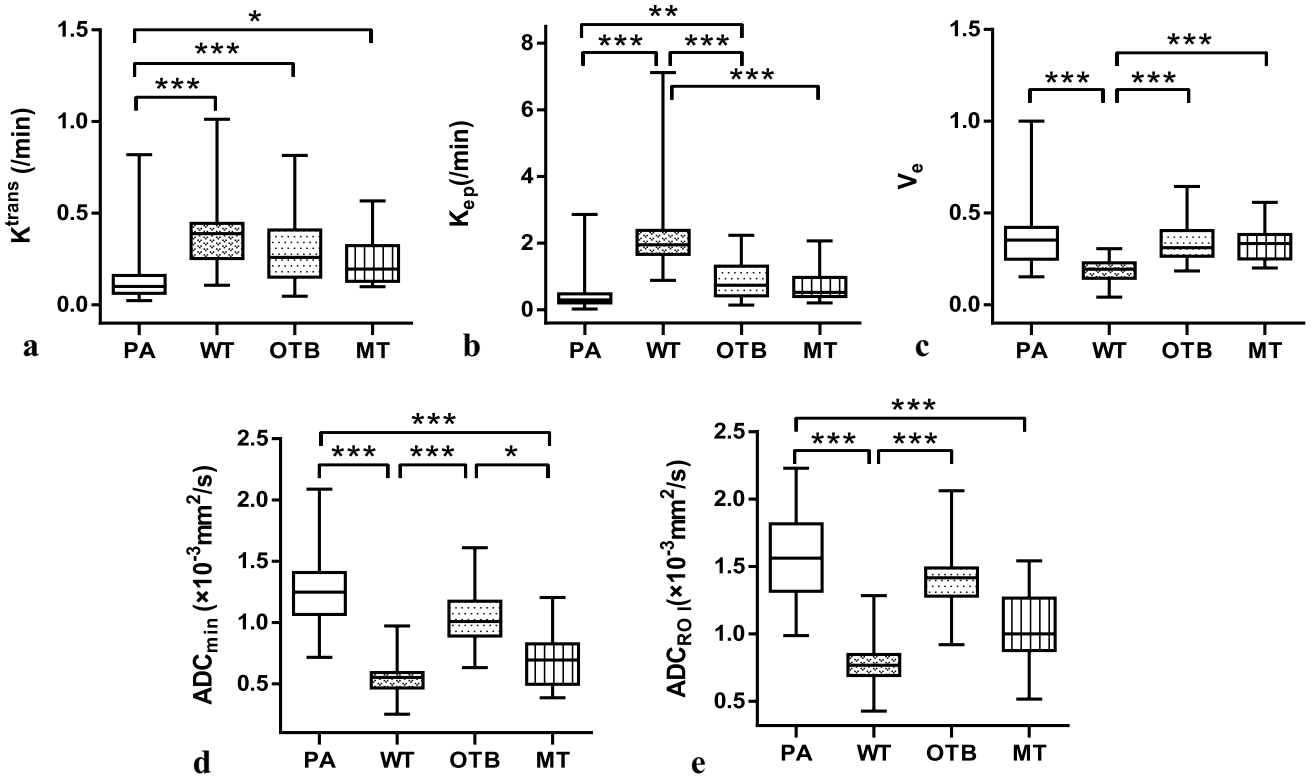

Fig. 1 Comparisons of the K^{trans} (**a**), K_{ep} (**b**), V_e (**c**), ADC_{ROI} (**d**), and ADC_{min} (**e**) values among four histological types of parotid lesions using the Dunn multiple comparison test with Bonferroni correction. *P < .05; **P < .01; ***P < .001. K^{trans} volume transfer constant, K_{ep} reverse rate constant, V_e fractional volume in the EES, ADC_{ROI} the apparent diffusion coefficient of corresponding ROI in DCE parameter measurements, ADC_{min} the minimum apparent diffusion coefficient of 5 small round ROI (ranging 0.03–0.05cm^2) within the former ROI in ADC_{ROI} measurement, *PA* pleomorphic adenomas, *OBN* other benign neoplasms, *WT* Warthin's tumors, *MT* malignant tumors

Table 3 Inter-reader and intra-reader reproducibility for measurements of K^{trans}, K_{ep}, V_e, ADC_{min}, and ADC_{ROI} values

Parameters	ICC (95% CI)	
	Inter-reader	Intra-reader
DCE parameters		
K^{trans}(/min)	0.925 (0.897–0.946)	0.955 (0.938–0.968)
K_{ep}(/min)	0.948 (0.928–0.962)	0.969 (0.957–0.978)
V_e	0.938 (0.915–0.955)	0.962 (0.947–0.972)
DWI parameters		
ADC_{min} (×10^{-3}mm^2/s)	0.932 (0.879–0.959)	0.966 (0.952–0.975)
ADC_{ROI} (×10^{-3}mm^2/s)	0.966 (0.953–0.976)	0.984 (0.978–0.989)

Data in parentheses are the 95% confidence interval

ICC intraclass correlation coefficient, *CI* confidence interval, K^{trans} volume transfer constant, K_{ep} reverse rate constant, V_e fractional volume in the EES, ADC_{ROI} the apparent diffusion coefficient of corresponding ROI in DCE parameter measurements, ADC_{min} the minimum apparent diffusion coefficient of 5 small round ROI (ranging 0.03–0.05 cm^2) within the former ROI in ADC_{ROI} measurement

Significances were found in ROC comparison between $K_{ep}+V_e$ and K_{ep} ($P=0.0217$) and between $K_{ep}+V_e$ and V_e ($P=0.0014$). As such, we used the combination of K_{ep} and V_e with the highest Youden index to discriminate WTs from the other three groups of PTs.

Following that, PAs and OBNs were grouped, since the mean ADC_{min} value was found lower in MTs than in both PAs and OBNs. The ROC analysis revealed that a cutoff ADC_{min} value of 0.826 yielded a sensitivity of 80.0%, a specificity of 92.3%, and an accuracy of 90.3% for distinguishing MTs from PAs and OBNs (Table 4 and Fig. 2b).

Finally, only PAs and OBNs remained to be differentiated. PAs showed higher K^{trans} and K_{ep} values than OBNs so that we used K^{trans} and K_{ep} to discriminate them. The ROC analyses demonstrated that a cutoff K^{trans} value of 0.185 yielded a sensitivity of 84.3% and a specificity of 70.4% and an accuracy of 79.5%; a cutoff K_{ep} value of 0.546 yielded a sensitivity of 82.4%, a specificity of 70.4%, and an accuracy of 78.2% (Table 4 and Fig. 2c). The AUC of K^{trans} was found higher than K_{ep} although it did not reach statistical significance ($P=0.1465$). In this way, a diagram of stepwise differential diagnostic was proposed for differentiating PAs, WTs, OBNs,

Table 4 Measurements of the threshold value, Youden index, sensitivity, specificity, PPV, NPV, accuracy, and AUC of RESOLVE-DWI and DCE-MRI parameters for differentiating parotid tumors

	TV	YI	Sensitivity (%)	Specificity (%)	PPV (%)	NPV (%)	Accuracy (%)	AUC	*P*
WTs ($n=52$) *vs.* PAs + OBNs + MTs ($n=93$)									
K_{ep}	> 1.016	0.781	94.2	83.9	76.6	96.3	87.6	0.940	.0217*
V_e	≤ 0.257	0.719	92.3	79.6	71.6	94.9	89.1	0.916	.0014*
$K_{ep} + V_e$	> 0.169	0.830	98.1	85	78.5	98.7	89.7	0.974	
MTs($n=15$) *vs.* PAs + OBNs($n=78$)									
ADC_{min}	≤ 0.826	0.723	80.0	96.2	80.0	96.0	93.6	0.913	
PAs ($n=51$) *vs.* OBNs ($n=27$)									
K^{trans}	≤ 0.185	0.547	84.3	70.4	84.3	70.4	79.5	0.804	0.1465
K_{ep}	≤ 0.546	0.527	82.4	70.4	84.0	67.9	78.2	0.767	

TV threshold value, *YI* youden index, *PPV* positive predictive value, *NPV* negative predictive value, *AUC* area under the curve, K^{trans} volume transfer constant, K_{ep} reverse rate constant, V_e fractional volume in the EES, ADC_{ROI} the apparent diffusion coefficient of corresponding ROI in DCE parameter measurements, ADC_{min} the minimum apparent diffusion coefficient of 5 small round ROI (ranging 0.03–0.05 cm^2) within the former ROI in ADC_{ROI} measurement, *PAs* pleomorphic adenomas, *OBNs* other benign neoplasms, *WTs* Warthin's tumors, *MTs* malignant tumors

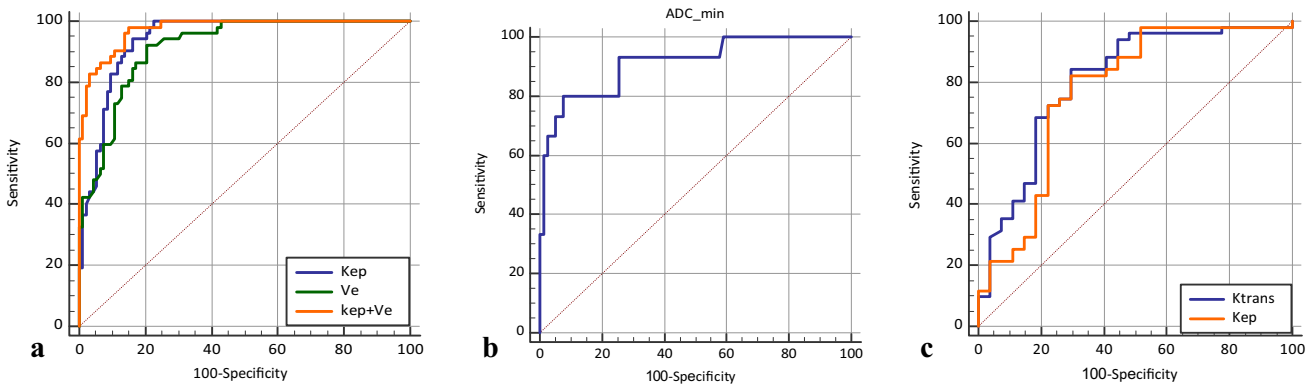

Fig. 2 (**a**) ROC curves of K_{ep}, V_e values and combination of K_{ep} and V_e for differentiating Warthin's tumors from the other three groups of parotid tumors, including, pleomorphic adenomas, other benign neoplasms and malignant tumors. (**b**) ROC curves of ADC_{min} values for distinguishing malignant tumors from pleomorphic adenomas and other benign neoplasms. (**c**) ROC curve of K^{trans} and K_{ep} for the discrimination of pleomorphic adenomas from other benign neoplasms. *ROC* receiver operating characteristic

and MTs (Fig. 3), rendering high accuracy of differential diagnosis of WTs, MTs, and PAs of 93.8, 89.0, and 82.1% respectively (Table 5).

Figures 4–5 showed representative cases.

Validation results

Table 5 also showed the validation results. When applying the stepwise differential protocol to 5 patients, the accuracy of differential diagnosis of WTs, MTs, and PAs were 100, 80, 80, and 80%.

Discussion

In this study, we utilized quantitative DCE-MRI parameters and RESOLVE-DWI in a stepwise discriminative method for the differential diagnosis of four histological types of PTs, including PAs, WTs, OBNs, and MTs. The DCE-MRI parameters of K^{trans}, K_{ep}, V_e, and ADC_{min} derived from RESOLVE-DWI are beneficial for this stepwise differentiation.

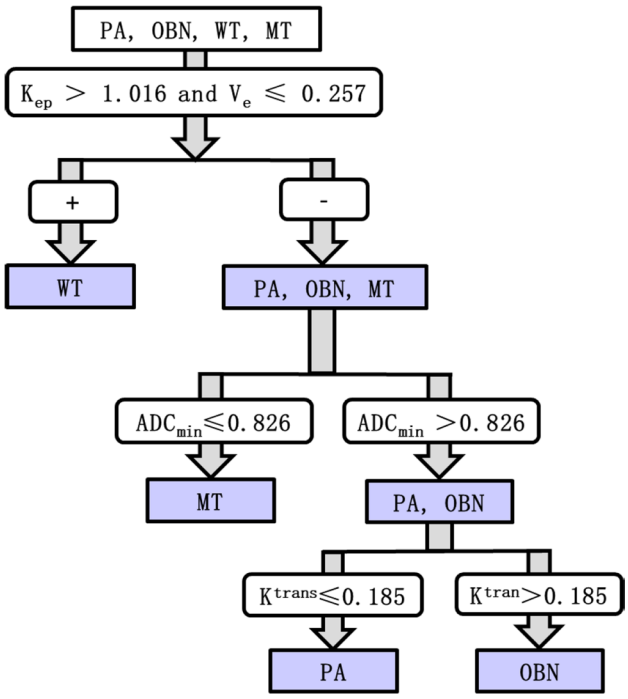

Fig. 3 Stepwise differentiation of four histological types of parotid tumors, including Warthin's tumors, malignant parotid tumors, pleomorphic adenomas, other benign neoplasms using RESOLVE-based ADC and IVIM parameters. *PA* pleomorphic adenomas, *OBN* other benign neoplasms, *WT* Warthin's tumors, *MT* malignant tumors

Table 5 Diagnostic accuracy with the combination of RESOLVE-DWI and DCE-MRI for the differentiation of parotid tumors

Tumor type	RESOLVE-DWI/DCE-MRI criteria				Diagnostic accuracy
	K_{ep}	V_e	ADC_{min}	K^{trans}	
WTs	> 1.016	≤ 0.257	-	-	93.8% (136/145)
MTs	≤ 1.016	> 0.257	≤ 0.826	-	89.0% (129/145)
PAs	≤ 1.016	> 0.257	> 0.826	≤ 0.185	82.1% (119/146)
OBNs	≤ 1.016	> 0.257	> 0.826	> 0.185	82.1% (119/146)
Validation study					
WTs	> 1.016	≤ 0.257	-	-	100% (4/5)
MTs	≤ 1.016	> 0.257	≤ 0.826	-	80% (4/5)
PAs	≤ 1.016	> 0.257	> 0.826	≤ 0.185	80% (4/5)
OBNs	≤ 1.016	> 0.257	> 0.826	> 0.185	80% (4/5)

K^{trans} volume transfer constant, K_{ep} reverse rate constant, V_e fractional volume in the EES, ADC_{min} the minimum apparent diffusion coefficient of 5 small round ROI (ranging 0.03–0.05 cm^2) within the former ROI in ADC_{ROI} measurement, *PA* pleomorphic adenomas, *OBN* other benign neoplasms, *WT* Warthin's tumors, *MT* malignant tumors

Quantitative DCE-MRI parameters, including K^{trans}, K_{ep}, and V_e, are useful in evaluating tumor permeability and angiogenesis, showing high efficacy in differentiating tumors in the head and neck [34–36]. K^{trans}, referring to the volume transfer constant, characterizes the effusion of contrast agent from the blood plasma into the EES [17]. It positively correlates with microvascular blood flow, microvessel density, and vascular permeability of diseased tissue. In this study, our findings showed that PAs had the lowest K^{trans} compared with WTs, OBNs, and MTs. These results were consistent with the previous studies reported by Patella et al. [23] and Xu et al. [25]. Histopathologically, PAs typically have fewer microvessels, resulting in low inflow rate of contrast agent (lowest K^{trans}). Unlike PAs, WTs usually have densely packed, capillary-like vessel network [37], which leads to a large amount of contrast agent influx. In MTs, vessel hyperplasia and abnormal angiogenesis are represented by leakage, vascular wall expansion, and cross-linking [38], which consequently leads to high permeability [39] and higher K^{trans}. Our results also showed higher K^{trans} in OBNs in comparison with PAs, which has not been reported yet. The considerable amount of basal cell adenomas (BCAs) in the groups of OBNs (18/27) may account for this difference. The most common solid type of BCAs was reported to have numerous endothelial-lined vessel with prominent small capillaries and venules [40]. This vascular-rich nature might explain the high K^{trans} of BCAs and thus increase the differences between PAs and OBNs. Hence, a low K^{trans} value may serve as an efficient indicator for diagnosing PAs. Additionally, our data showed relatively higher K^{trans} of WTs compared with MTs although it did not reach statistical significance, which was in accordance with the previous study of Xu et al. [25]. Regardless, our findings hinted that K^{trans} value may aid in distinguishing PAs from WTs, OBNs and MTs, and WTs from MTs.

K_{ep} (reverse rate constant), qualifying the outflux of contrast agent from the EES back to the plasma, correlates positively with microvascular blood flow, microvessel density, and vascular permeability of the diseased tissue as well [41]. Tumors with abundant microvessels increase vascular permeability by offering more vascular channel available for the outflow of contrast agent from EES. V_e is the volume of the EES per unit volume of the contrast agent in the tissue, which relates positively to tissue necrosis or amount of stroma and negatively to tumor cellularity [41, 42]. Previous studies demonstrated that tumors with a high cellularity-stromal ratio had a high washout ratio [12]. Similarly, we speculate that the high cellularity-stromal ratio may result in limited EES and less retention of contrast agents, which consequently relates to a high K_{ep} and low V_e. Our study demonstrated that WTs showed a highest K_{ep} and lowest V_e compared with PAs, OBNs, and MTs, which was in line with the studies of Xu et al. [25] and Yabuuchi et al. [43]. In histopathology, WTs were densely packed with lymphoid cells [44] and displayed with capillary-like vessel network, resulting in narrow EES and less retention of contrast agents. Thus, it is not surprising to find a high K_{ep} and low V_e in WTs.

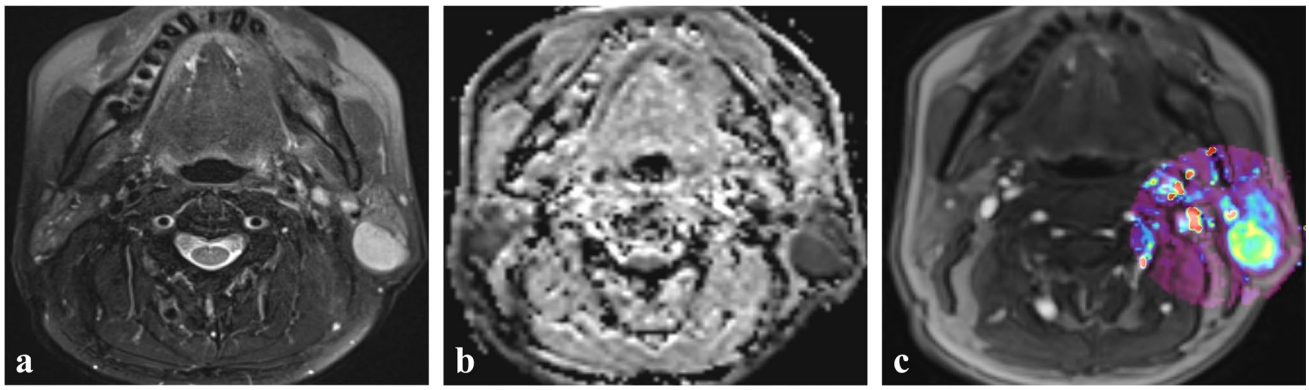

Fig. 4 Warthin's tumor in a 57-year-old man. A mass locating in the left parotid gland demonstrated hyperintensity on T2WI (**a**). On ADC images (**b**), the mass appeared obviously hypointense with ADC_{ROI} value of 0.661 and ADC_{min} value of 0.559 mm^2/s, respectively. A color-coded K^{trans} map based on DCE-MRI (**c**) was obtained, yielding the mean K^{trans}, K_{ep}, and V_e values of 0.299/min, 1.649/min and 0.182, respectively

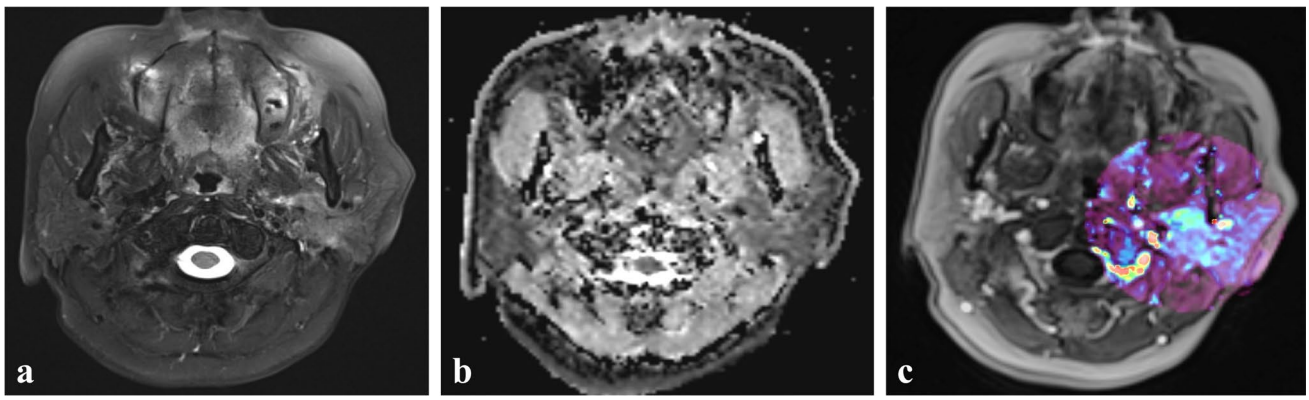

Fig. 5 A 55-year-old woman with a mucoepidermoid carcinoma. A mass was located in the left parotid gland demonstrating hyperintensity on T2WI (**a**). On ADC images (**b**), the mass appeared obviously hypointense with ADC_{ROI} value of 1.048 and ADC_{min} value of 0.689mm^2/sec, respectively. A color-coded K^{trans} map based on DCE-MRI (**c**) was obtained, showing the mass with the mean K^{trans}, K_{ep}, and V_e values of 0.316/min, 0.960/min, and 0.329, respectively

Contrarily, PAs have less microvessels and richer stroma compared with WTs, which may result in a lower K_{ep} and higher V_e. Moreover, lower cellularity-stroma grade and excess mucous content within some MTs (such as mucoepidermoid carcinoma) can decrease K_{ep} and increase V_e, which may finally lead to a lower K_{ep} and higher V_e in MTs compared with WTs in our study. Therefore, K_{ep} and V_e could be taken as promising indicators for diagnosing WTs. Notably, our study found that the K_{ep} value of OBNs was significantly higher than that of PAs, which has not been described in previous studies. The considerable number of BCAs in the groups of OBNs (18/27) may again explain the difference. BCAs have higher cellularity-stromal grade than PAs for their lacking of myxochondroid stroma and mesenchymal mucin [45], and the prominent small venules within the numerous endothelial-lined vascular channels in BCAs [40] increase K_{ep} because of more contrast agent diffusion back to the plasma from the EES. Hence, a low K_{ep} value may help to differentiate PAs.

RESOLVE-DWI is a novel technique that reduces spatial distortion and performs a nonlinear phase correction and control of the real-time reacquisition of unusable data that cannot be corrected [20]. Few research on the application of RESOLVE-DWI in differentiating PTs is currently available. In this study, the ADC_{ROI} and ADC_{min} values of WTs and MTs were both lower than that of PAs and OBNs. The high cellularity in MTs and WTs might account for lower ADC values, while the relative abundance of myxoid and chondroid stroma explaining higher ADC values in PAs [15]. These results were in agreement with the previous studies [15, 18, 46]. Interestingly, although MTs had lower ADC values than OBNs, the difference of ADC_{ROI} values between OBNs and MTs did not reach a statistical significance as ADC_{min} did. The possible reason may be as follows:

malignancies are often heterogeneous and some MTs (such as mucoepidermoid carcinoma) contain abundant microscopic areas of necrosis or mucus which might attributed to a high ADC_{ROI} value in MTs compared with ADC_{min} [47]. Nevertheless, a lower ADC value might assist in the differentiation of WTs and MTs from PAs and OBNs.

ROC curve analyses demonstrated that K_{ep} and V_e values yielded high sensitivity and specificity for differentiating WTs from PAs, MTs, and OBNs. The diagnostic performance can be significantly improved after combination of K_{ep} and V_e value with the highest sensitivity, specificity, and accuracy for distinguishing WTs from PAs, OBNs, and MTs, suggesting the combination of K_{ep} and V_e may serve as the optimal imaging biomarker for diagnosing WTs. Moreover, ADC_{min} provides a high sensitivity, specificity, and accuracy, for distinguishing MTs from PAs and OBNs. Furthermore, our study found that K^{trans} provide a higher sensitivity (84.3%) for further discrimination of PAs and OBNs (accuracy = 79.5%) than K_{ep} although it did not reach statistical significance ($P = 0.1465$). A larger homogeneous sample might yield more pronounced and significant results. Consequently, in this stepwise protocol, the combination of quantitative DCE-MRI and RESOLVE-DWI can effectively discriminate these four different histological types of PTs with high accuracy of 93.8, 89.0, and 82.1% respectively for differentiating WTs, MTs, and PAs in the initial algorithm development study and 100, 80, 80, and 80% in the validation study. We speculate that less overlap of K_{ep}, V_e, and ADC values might account for high accuracy in our stepwise discrimination. Previous studies [25, 43] also revealed that K_{ep}, V_e, and ADC values played an important part in improving accuracy of PT discrimination. Xu et al. [25] demonstrated that the combination of TIC pattern and V_e provided highest diagnostic accuracy of 75% followed by the combination with ADC. Yabuuchi et al. [43] found when K_{ep} and D, the only two parameters in their decision-tree algorithm were added to and TIC pattern, the accuracy for differentiation of benign and malignant PTs raised to 93%. These results were in agreement with our study. In our study, K^{trans} played an important role in the last step of stepwise discrimination and improving the overall accuracy. However, K^{trans} was not useful for PTs discrimination reported in the study of Yabuuchi et al. [43]; and K^{trans} between PAs and OBNs was also insignificant in the study of Xu et al. [25]. The discrepancy between our results and these previous studies might be caused by the different constituting pathological types in OBNs and MTs between those studies and ours. Regardless, our validation study confirmed the potential of K^{trans} in improving the discrimination accuracy in PTs.

Our study still had several limitations. First, as a retrospective study, a selection bias was unavoidable. Second, the sample size of OBNs and MTs was relatively small, and they had a variety of pathological types with imbalance proportion, which might affect the results. The sample number for validation study was inadequate. Therefore, further prospective studies with a larger sample size are required to confirm our findings. Third, the manual definition of ROI may bring inevitable potential sampling bias and small ROIs for ADC_{min} measurements would affect the consistent acquisition of reliable values. A whole-volume ROI may supply added information about the tumor heterogeneity in the future study. Last, our proposed stepwise protocol in this study was relatively complicated. Further optimization and verification are still required.

In conclusion, quantitative DCE-MRI and RESOLVE-DWI are beneficial for the characterization of different histological types of PTs including PAs, WTs, OBNs, and MTs. The combination of these two techniques in a stepwise protocol can effectively discriminate these four histological types of PTs.

Funding This study was supported by the Startup Fund for scientific research of Fujian Medical University (No. 2019QH1105).

Declarations

Conflict of interest The authors declare that they have no conflict of interest.

Ethical approval All procedures performed in studies involving human participants were in accordance with the ethical standards of the institutional and/or national research committee and with the 1964 Helsinki declaration and its later amendments or comparable ethical standards.

For this type of study formal consent is not required.

Informed consent The study was approved by our institutional review committee. Due to the retrospective nature of the investigation, informed consent has been waived for this study.

References

1. Upton DC, McNamar JP, Connor NP, Harari PM, Hartig GK (2007) Parotidectomy: ten-year review of 237 cases at a single institution. Otolaryngol Head Neck Surg 136(5):788–792
2. Freling N, Crippa F, Maroldi R (2016) Staging and follow-up of high-grade malignant salivary gland tumours: the role of traditional versus functional imaging approaches - a review. Oral Oncol 60:157–166
3. Witt RL (2002) The significance of the margin in parotid surgery for pleomorphic adenoma. Laryngoscope 112(12):2141–2154
4. Sciubba JJ, Brannon RB (1982) Myoepithelioma of salivary glands: report of 23 cases. Cancer 49(3):562–572
5. Bradley PT, Paleri V, Homer JJ (2012) Consensus statement by otolaryngologists on the diagnosis and management of benign parotid gland disease. Clin Otolaryngol 37(4):300–304
6. Zbaren P, Vander Poorten V, Witt RL, Woolgar JA, Shaha AR, Triantafyllou A, Takes RP, Rinaldo A, Ferlito A (2013) Pleomorphic adenoma of the parotid: formal parotidectomy or limited surgery? Am J Surg 205(1):109–118

7. Magnano M, Gervasio CF, Cravero L, Machetta G, Lerda W, Beltramo G, Orecchia R, Ragona R, Bussi M (1999) Treatment of malignant neoplasms of the parotid gland. Otolaryngol Head Neck Surg 121(5):627–632
8. Prades JM, Oletski A, Faye MB, Dumollard JM, Timoshenko AP, Veyret C, Peoc'h M, Martin C (2007) Parotid gland masses: diagnostic value of MR imaging with histopathologic correlations. Morphologie 91(292):44–51
9. Yousem DM, Kraut MA, Chalian AA (2000) Major salivary gland imaging. Radiology 216(1):19–29
10. Freling NJ, Molenaar WM, Vermey A, Mooyaart EL, Panders AK, Annyas AA, Thijn CJ (1992) Malignant parotid tumors: clinical use of MR imaging and histologic correlation. Radiology 185(3):691–696
11. Elmokadem AH, Abdel Khalek AM, Abdel Wahab RM, Tharwat N, Gaballa GM, Elata MA, Amer T (2019) Diagnostic accuracy of multiparametric magnetic resonance imaging for differentiation between parotid neoplasms. Can Assoc Radiol J 70(3):264–272
12. Yabuuchi H, Fukuya T, Tajima T, Hachitanda Y, Tomita K, Koga M (2003) Salivary gland tumors: diagnostic value of gadolinium-enhanced dynamic MR imaging with histopathologic correlation. Radiology 226(2):345–354
13. Kitamoto E, Chikui T, Kawano S, Ohga M, Kobayashi K, Matsuo Y, Yoshiura T, Obara M, Honda H, Yoshiura K (2015) The application of dynamic contrast-enhanced MRI and diffusion-weighted MRI in patients with maxillofacial tumors. Acad Radiol 22(2):210–216
14. Yabuuchi H, Matsuo Y, Kamitani T, Setoguchi T, Okafuji T, Soeda H, Sakai S, Hatakenaka M, Nakashima T, Oda Y et al (2008) Parotid gland tumors: can addition of diffusion-weighted MR imaging to dynamic contrast-enhanced MR imaging improve diagnostic accuracy in characterization? Radiology 249(3):909–916
15. Habermann CR, Arndt C, Graessner J, Diestel L, Petersen KU, Reitmeier F, Ussmueller JO, Adam G, Jaehne M (2009) Diffusion-weighted echo-planar MR imaging of primary parotid gland tumors: is a prediction of different histologic subtypes possible? AJNR Am J Neuroradiol 30(3):591–596
16. Coudert H, Mirafzal S, Dissard A, Boyer L, Montoriol PF (2021) Multiparametric magnetic resonance imaging of parotid tumors: a systematic review. Diagn Interv Imaging 102(3):121–130
17. Chikui T, Obara M, Simonetti AW, Ohga M, Koga S, Kawano S, Matsuo Y, Kamintani T, Shiraishi T, Kitamoto E et al (2012) The principal of dynamic contrast enhanced MRI, the method of pharmacokinetic analysis, and its application in the head and neck region. Int J Dent 2012:480659
18. Sumi M, Van Cauteren M, Sumi T, Obara M, Ichikawa Y, Nakamura T (2012) Salivary gland tumors: use of intravoxel incoherent motion MR imaging for assessment of diffusion and perfusion for the differentiation of benign from malignant tumors. Radiology 263(3):770–777
19. Koyasu S, Iima M, Umeoka S, Morisawa N, Porter DA, Ito J, Le Bihan D, Togashi K (2014) The clinical utility of reduced-distortion readout-segmented echo-planar imaging in the head and neck region: initial experience. Eur Radiol 24(12):3088–3096
20. Porter DA, Heidemann RM (2009) High resolution diffusion-weighted imaging using readout-segmented echo-planar imaging, parallel imaging and a two-dimensional navigator-based reacquisition. Magn Reson Med 62(2):468–475
21. Leach MO, Morgan B, Tofts PS, Buckley DL, Huang W, Horsfield MA, Chenevert TL, Collins DJ, Jackson A, Lomas D et al (2012) Imaging vascular function for early stage clinical trials using dynamic contrast-enhanced magnetic resonance imaging. Eur Radiol 22(7):1451–1464
22. Tofts PS, Brix G, Buckley DL, Evelhoch JL, Henderson E, Knopp MV, Larsson HB, Lee TY, Mayr NA, Parker GJ et al (1999) Estimating kinetic parameters from dynamic contrast-enhanced T(1)-weighted MRI of a diffusable tracer: standardized quantities and symbols. J Magn Reson Imaging 10(3):223–232
23. Patella F, Franceschelli G, Petrillo M, Sansone M, Fusco R, Pesapane F, Pompili G, Ierardi AM, Saibene AM, Moneghini L et al (2018) A multiparametric analysis combining DCE-MRI- and IVIM -derived parameters to improve differentiation of parotid tumors: a pilot study. Future Oncol 14(28):2893–2903
24. Patella F, Sansone M, Franceschelli G, Tofanelli L, Petrillo M, Fusco M, Nicolino GM, Buccimazza G, Fusco R, Gopalakrishnan V et al (2020) Quantification of heterogeneity to classify benign parotid tumors: a feasibility study on most frequent histotypes. Future Oncol 16(12):763–778
25. Xu Z, Zheng S, Pan A, Cheng X, Gao M (2019) A multiparametric analysis based on DCE-MRI to improve the accuracy of parotid tumor discrimination. Eur J Nucl Med Mol Imaging 46(11):2228–2234
26. Park JY, Shin HJ, Shin KC, Sung YS, Choi WJ, Chae EY, Cha JH, Kim HH (2015) Comparison of readout segmented echo planar imaging (EPI) and EPI with reduced field-of-VIew diffusion-weighted imaging at 3t in patients with breast cancer. J Magn Reson Imaging 42(6):1679–1688
27. Yeom KW, Holdsworth SJ, Van AT, Iv M, Skare S, Lober RM, Bammer R (2013) Comparison of readout-segmented echo-planar imaging (EPI) and single-shot EPI in clinical application of diffusion-weighted imaging of the pediatric brain. AJR Am J Roentgenol 200(5):W437-443
28. Xu X, Wang Y, Hu H, Su G, Liu H, Shi H, Wu F (2017) Readout-segmented echo-planar diffusion-weighted imaging in the assessment of orbital tumors: comparison with conventional single-shot echo-planar imaging in image quality and diagnostic performance. Acta Radiol 58(12):1457–1467
29. Zhao M, Liu Z, Sha Y, Wang S, Ye X, Pan Y, Wang S (2016) Readout-segmented echo-planar imaging in the evaluation of sinonasal lesions: a comprehensive comparison of image quality in single-shot echo-planar imaging. Magn Reson Imaging 34(2):166–172
30. Wisner DJ, Rogers N, Deshpande VS, Newitt DN, Laub GA, Porter DA, Kornak J, Joe BN, Hylton NM (2014) High-resolution diffusion-weighted imaging for the separation of benign from malignant BI-RADS 4/5 lesions found on breast MRI at 3T. J Magn Reson Imaging 40(3):674–681
31. Ma G, Zhu LN, Su GY, Hu H, Qian W, Bu SS, Xu XQ, Wu FY (2018) Histogram analysis of apparent diffusion coefficient maps for differentiating malignant from benign parotid gland tumors. Eur Arch Otorhinolaryngol 275(8):2151–2157
32. Zhang Z, Song C, Zhang Y, Wen B, Zhu J, Cheng J (2019) Apparent diffusion coefficient (ADC) histogram analysis: differentiation of benign from malignant parotid gland tumors using readout-segmented diffusion-weighted imaging. Dentomaxillofac Radiol 48(7):20190100
33. Alibek S, Zenk J, Bozzato A, Lell M, Grunewald M, Anders K, Rabe C, Iro H, Bautz W, Greess H (2007) The value of dynamic MRI studies in parotid tumors. Acad Radiol 14(6):701–710
34. Gaddikeri S, Hippe DS, Anzai Y (2016) Dynamic Contrast-Enhanced MRI in the Evaluation of Carotid Space Paraganglioma versus Schwannoma. J Neuroimaging 26(6):618–625
35. Lee FK, King AD, Ma BB, Yeung DK (2012) Dynamic contrast enhancement magnetic resonance imaging (DCE-MRI) for differential diagnosis in head and neck cancers. Eur J Radiol 81(4):784–788
36. Yu JY, Zhang D, Huang XL, Ma J, Yang C, Li XJ, Xiong H, Zhou B, Liao RK, Tang ZY (2020) Quantitative analysis of DCE-MRI and RESOLVE-DWI for differentiating nasopharyngeal carcinoma from nasopharyngeal lymphoid hyperplasia. J Med Syst 44(4):75

37. Woo SH, Choi DS, Kim JP, Park JJ, Joo YH, Chung PS, Kim BY, Ko YH, Jeong HS, Kim HJ (2013) Two-phase computed tomography study of warthin tumor of parotid gland: differentiation from other parotid gland tumors and its pathologic explanation. J Comput Assist Tomogr 37(4):518–524
38. Furuya M, Yonemitsu Y (2008) Cancer neovascularization and proinflammatory microenvironments. Curr Cancer Drug Targets 8(4):253–265
39. Jain RK (2005) Normalization of tumor vasculature: an emerging concept in antiangiogenic therapy. Science 307(5706):58–62
40. Triest WE, Fried MP, Stanievich JF (1983) Membranous basal cell adenoma of the hypopharynx. Arch Otolaryngol 109(11):774–777
41. Ahn SJ, An CS, Koom WS, Song HT, Suh JS (2011) Correlations of 3T DCE-MRI quantitative parameters with microvessel density in a human-colorectal-cancer xenograft mouse model. Korean J Radiol 12(6):722–730
42. Kim SH, Lee HS, Kang BJ, Song BJ, Kim HB, Lee H, Jin MS, Lee A (2016) Dynamic contrast-enhanced MRI perfusion parameters as imaging biomarkers of angiogenesis. PLoS One 11(12):e0168632
43. Yabuuchi H, Kamitani T, Sagiyama K, Yamasaki Y, Hida T, Matsuura Y, Hino T, Murayama Y, Yasumatsu R, Yamamoto H (2020) Characterization of parotid gland tumors: added value of permeability MR imaging to DWI and DCE-MRI. Eur Radiol 30(12):6402–6412
44. Ikeda M, Motoori K, Hanazawa T, Nagai Y, Yamamoto S, Ueda T, Funatsu H, Ito H (2004) Warthin tumor of the parotid gland: diagnostic value of MR imaging with histopathologic correlation. AJNR Am J Neuroradiol 25(7):1256–1262
45. Lee JY, Kim HJ, Kim YK, Cha J, Kim ST (2019) Basal cell adenoma and myoepithelioma of the parotid gland: patterns of enhancement at two-phase CT in comparison with Warthin tumor. Diagn Interv Radiol 25(4):285–290
46. Eida S, Sumi M, Sakihama N, Takahashi H, Nakamura T (2007) Apparent diffusion coefficient mapping of salivary gland tumors: prediction of the benignancy and malignancy. AJNR Am J Neuroradiol 28(1):116–121
47. Celebi I, Mahmutoglu AS, Ucgul A, Ulusay SM, Basak T, Basak M (2013) Quantitative diffusion-weighted magnetic resonance imaging in the evaluation of parotid gland masses: a study with histopathological correlation. Clin Imaging 37(2):232–238